12-4-2017

A Development and Application of the Finite Element Method for Predicting the Aggregate Behavior of a Large System based on Classical Microscopic Assumptions

Juan Gabriel Alonso Guzman

Follow this and additional works at: https://louis.uah.edu/honors-capstones

A Development and Application of the Finite Element Method for Predicting the Aggregate Behavior of a Large System based on Classical Microscopic Assumptions

by

Juan Gabriel Alonso Guzman

An Honors Capstone

submitted in partial fulfillment of the requirements

for the Honors Diploma

to

The Honors College
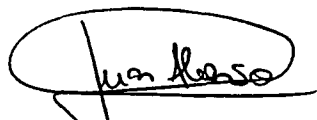
of

The University of Alabama in Huntsville

December 4th, 2017

Honors Capstone Director: Dr. Anthony Hester

Adjunct Professor of the Mathematical Sciences Department at UAH

(signature)	12/07/17
Student	Date
(signature)	2017-Dec-07
Director	Date
(signature)	12/7/17
Department Chair	Date
(signature)	12/11/17
Honors College Dean	Date

Honors Thesis Copyright Permission

This form must be signed by the student and submitted as a bound part of the thesis.

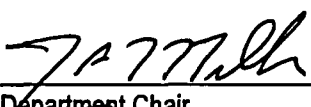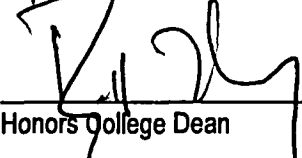In presenting this thesis in partial fulfillment of the requirements for Honors Diploma or Certificate from The University of Alabama in Huntsville, I agree that the Library of this University shall make it freely available for inspection. I further agree that permission for extensive copying for scholarly purposes may be granted by my advisor or, in his/her absence, by the Chair of the Department, Director of the Program, or the Dean of the Honors College. It is also understood that due recognition shall be given to me and to The University of Alabama in Huntsville in any scholarly use which may be made of any material in this thesis.

Juan G. Alonso Guzmán

Student Name (printed)

[signature]

Student Signature

12|07|17

Date

A Development and Application of the Finite Element Method for Predicting the Aggregate Behavior of a Large System based on Classical Microscopic Assumptions

Juan G Alonso Guzmán   Dr Anthony Hester

December 4, 2017

Abstract

In this paper, we first provide a detailed development of the Finite Element Method (FEM) from its abstract mathematical foundation to its application in continuum mechanics, namely solving Cauchy's First Law of Motion (CFLM). Throughout this process, we are careful in proving all the necessary theorems and defining the appropriate physical quantities to ensure a standard of rigor and coherence lacking in the current literature concerning this topic. We then test the software tools we have developed using the theory in terms of accuracy and efficiency, and comment on our results.

1

Contents

1 Introduction

In this paper, we present the first step in a much broader and long-term research effort of modeling quantum systems. In particular, the content presented here falls under the realm of continuum mechanics, since this is precisely the limiting behavior of quantum systems with an increasingly large number of particles. As a preliminary outline, we first discuss a necessary component mathematical theory, the Finite Element Method (FEM). This method is a numerical approach to solving partial differential equations. We will then give a brief overview of the physical quantities of interests in situations involving the linear deformation of rigid bodies, and derive Cauchy's First Law of Motion (CFLM), which could be regarded as the overarching formula relating the forces applied on a body with its resulting deformation. We later move on to present a couple simulations performed with our own structural analysis software aimed at testing its accuracy and efficiency, and offer some commentary on our findings. Finally, we conclude with a few thoughts on some avenues of progress when moving forward with this project.

2 Mathematical Theory

In order to study continuum mechanics properly, one must first become well-versed in the mathematical field of differential geometry. Part of achieving a solid foundation in said area of mathematics comes through acquiring a good understanding of abstract (linear) algebra (i.e. Hilbert/Banach Spaces, tensor theory, etc). Furthermore, the unavoidable time-dependent problems that arise in this branch of physics, and any other for that matter, can only be solved with the pertinent knowledge of differential equations (both ordinary and partial). In many cases, however, complicated problems have no closed-form (analytical) solution and mathematicians/physicists must then resort to numerical approaches in order to find a "good enough" (approximated) solution. In this section, we will prove some preliminary theorems, state a few equivalent forms of differential equations, and then briefly discuss one of the numerical schemes for solving them, namely the Finite Element Method, which is currently very popular in both academia and industry.

2.1 Preliminary Theorems

We begin with a, relatively simple, yet extremely important lemma.

Lemma 2.1 *Let $\tau : \mathbb{R}^3 \to \mathbb{R}^{3\times3}$ and $\phi : \mathbb{R}^3 \to \mathbb{R}^3$ be differentiable. If for any representation of τ, we have that $\tau_{ij} = \tau_{ji}, \forall 1 \leq i, j \leq 3$ then*

$$\nabla \cdot (\tau\phi) = (\nabla \cdot \tau) \cdot \phi + \tau : \nabla\phi.$$

Proof: Let $\tau = [\tau_{ij}]$ and $\phi = [\phi_j]$. Then, using Einstein's summation convention and the product rule for derivatives,

$$\nabla \cdot (\tau\phi) = \nabla \cdot (\tau^{\mathrm{T}}\phi) = \frac{\partial}{\partial x_i}(\tau_{ji}\phi_j) = \frac{\partial \tau_{ji}}{\partial x_i}\phi_j + \tau_{ji}\frac{\partial \phi_j}{\partial x_i} = (\nabla \cdot \tau) \cdot \phi + \tau : \nabla\phi.$$

∎

Next, we show a slightly more complicated, yet equally valuable, lemma.

Lemma 2.2 *Let $L : X \to X$ be a bounded, Hermitian mapping on the inner product space X, and $f \in X$. Define $\Pi : X \to \mathbb{R}$ as*

$$\Pi(x) = \langle Lx, x \rangle - 2\langle f, x \rangle.$$

Then Π is Fréchet differentiable, and $u \in X$ is a critical point of Π (i.e. $D\Pi(u) = 0$) if and only if $Lu = f$.

Proof: First we must show that Π is indeed differentiable, by showing that

$$\Pi(x+h) - \Pi(x) = A(h) + \mathcal{O}(h)$$

where $A(= D\Pi)$ is some bounded linear operator.

$$
\begin{aligned}
\Pi(x+h) - \Pi(x) &= \langle L(x+h), x+h \rangle - 2\langle f, x+h \rangle - (\langle Lx, x \rangle - 2\langle f, x \rangle) \\
&= \langle Lx - 2f, h \rangle + \langle Lh, x \rangle + \langle Lh, h \rangle && \text{[Linearity of } L\text{]} \\
&= \langle Lx - 2f, h \rangle + \langle Lx, h \rangle + \langle Lh, h \rangle && \text{[}L \text{ is Hermitian]} \\
&= 2\langle Lx - f, h \rangle + \langle Lh, h \rangle
\end{aligned}
$$

Now, L is bounded. Therefore,

$$|\langle Lh, h \rangle| \leq \|L\| \cdot \|h\|^2$$

and $2\langle Lx - f, h \rangle$ is linear (in h) and bounded through Cauchy-Schwarz. Hence,

$$D\Pi(x) = 2\langle Lx - f, \cdot \rangle$$

Now, for the equivalence statement:

$$
\begin{aligned}
D\Pi(u) = 0 &\iff 2\langle Lu - f, \cdot \rangle = 0 \\
&\iff \langle Lu - f, \cdot \rangle = 0 \\
&\iff Lu - f = 0 \\
&\iff Lu = f
\end{aligned}
$$

∎

We continue with an essential theorem, stating the equivalence between differential and integral equations, which later on turns out to be of key importance for our purpose [1]. Moreover, under the appropriate conditions, a third equivalent form of these functional equations is provided.

4

Theorem 2.3 *Let $L : X \to X$ be a mapping on the inner product space X, and $f \in X$. Then, the following are equivalent:*

1. u solves the equation $Lx = f$.

2. u satisfies

$$a(u, x) = \langle f, x \rangle,$$

$\forall x \in X$ where $a(u, x) = \langle Lu, x \rangle$.

If, in addition, L is Hermitian, positive-definite, and bounded, then the previous statements are equivalent to the following:

3. u minimizes the quadratic functional

$$\Pi(x) = \langle Lx, x \rangle - 2\langle f, x \rangle = a(x, x) - 2\langle f, x \rangle.$$

Proof: $(1) \Rightarrow (2)$ Since $Lu = f$, then

$$a(u, x) = \langle Lu, x \rangle = \langle f, x \rangle, \qquad \forall x \in X$$

$(2) \Rightarrow (1)$ Similarly,

$$\langle Lu, x \rangle = a(u, x) = \langle f, x \rangle, \qquad \forall x \in X$$
$$\implies \langle Lu - f, x \rangle = 0, \qquad \forall x \in X$$
$$\implies \|Lu - f\|^2 = 0 \implies Lu = f$$

$(1) \Leftrightarrow (3)$ It follows from lemma 2.2 that u is a critical point of Π. We now have to show that it is actually a minimum. So, for any $h \in X$

$$
\begin{aligned}
\Pi(u + h) &= \langle L(u + h), x + h \rangle - 2\langle f, u + h \rangle \\
&= \langle Lu, u \rangle + \langle Lu, h \rangle + \langle Lh, u \rangle + \langle Lh, h \rangle - 2\langle f, u \rangle - 2\langle f, h \rangle \\
&= \langle Lu, u \rangle - 2\langle f, u \rangle + 2\langle Lu, h \rangle - 2\langle f, h \rangle + \langle Lh, h \rangle && [L \text{ is Hermitian}] \\
&= \Pi(u) + \langle Lh, h \rangle && [Lu = f] \\
&\geq \Pi(u) && [\langle Lh, h \rangle \geq 0]
\end{aligned}
$$

∎

If L is some "nice" differential operator on the pertinent Sobolev Space[1], X, then it is easily seen how the quadratic functional form can be a helpful characterization when attempting to solve the differential equation $Lu = f$. Nonetheless, we shall also explore later in this paper how minimizing this $\Pi(x)$ provides some insight into the underlying physical laws when applied to the proper context. Now, we delve straight into a general overview of the FEM.

---

[1] That is, some function space equipped with an L^p-norm defined not just on the function itself but also on some combination of its derivatives (in the weak sense) up to a certain order.

2.2 The Finite Element Method

Finite element analysis allows for the approximation of solutions to PDE's via the following steps [2]:

1. Identify a function (inner product) space X that contains the solution to the PDE.

2. Transform the PDE into a variational problem

$$a(u, x) = \langle f, x \rangle, \qquad \forall x \in X,$$

   involving a coercive, bilinear form $a : X \times X \to \mathbb{R}$, whose solution u solves the PDE (i.e. convert the differential equation to an integral equation).

3. Select a suitable finite dimensional subspace, $H \leq X$, which will allow for a "good" approximation of the true solution.

4. Solve the corresponding variational problem in H

$$a(u, x) = \langle f, x \rangle, \qquad \forall x \in H, \tag{1}$$

   through a system of linear equations. This can be done by selecting a basis $\{e_k\}_{k=1}^n$ for H to then convert the previously obtained integral equation into a matrix equation.

$$\langle f, e_i \rangle = a\left(\sum_j u_j e_j, e_i \right) = \sum_j a(e_j, e_i) u_j, \quad \text{or} \quad AU = F,$$

where $A_{ij} = a(e_j, e_i)$, $U_j = u_j$, and $F_i = \langle f, e_i \rangle$.

3 Physical Application

The Finite Element Method has numerous applications nowadays, one of which is solving Cauchy's First Law of Motion (CFLM) for rigid bodies in the field of continuum mechanics. In this section, we first present the main physical quantities and equations that describe the deformations of rigid bodies under the influence of external forces [3], and then we give a detailed explanation of how to specifically implement the FEM to solve CFLM.

3.1 Continuum Mechanics

Suppose we have a three-dimensional continuum body, $\Omega \subset \mathbb{R}^3$, under the influence of some inner body forces (per unit volume), $f_B(x, y, z)$, surface forces (per unit area), $f_S(x, y, z)$, and possibly some concentrated loads, $R_C(x, y, z)^2$. Then these forces will

---

[2]These represent forces applied on a very small patch of surface, and hence are idealized as forces applied at a specific point.

cause some deformation[3] (perceivable or not), $u(x, y, z)$, measured as a displacement at each point of the body.

Raw displacements can sometimes be deceiving. For example, a mm magnitude displacement may result negligible for a large-scale structure, like a bridge or building, whereas it may render small, precise pieces of equipment useless, such as simple bolts and screws. Moreover, different pieces of equipment are more prone to deform in one direction than another. The same amount of force it takes to considerably bend a metal cantilever attached to the wall at a single end may prove futile in trying to stretch the cantilever along its length axis. For these reasons, the quantity of elastic strain, $\varepsilon : \Omega \to \mathbb{R}^{3 \times 3}$, is defined as

$$\varepsilon(u)(x, y, z) = \frac{1}{2} \left(\nabla u + \nabla^T u \right), \qquad \forall (x, y, z) \in \Omega,$$

serving as a sort of "percentage displacements", which could originate from stretching, bending, twisting, etc. A couple of important facts to point out about elastic strain is that, in the physical context, it is unit-less, and, in the mathematical context, it is a Hermitian (and in the real case, symmetric) operator, which simplifies the development of the theory and its posterior application.

Along with the displacements and strains, we introduce the Cauchy Stress Tensor[4], σ, which for any point inside the body, maps the unit normal vector, $\hat{n}$, at some fixed cross section of the body containing that point, to the stress vector $T(\hat{n})$ on that same point (see figure 1). That is

$$T(\hat{n})(x, y, z) = \sigma(x, y, z) \cdot \hat{n}, \qquad \forall (x, y, z) \in \Omega.$$

The stress vector can be thought of as the net effect that the particles on the opposite side of the cross section have on the chosen particle in space. In addition, T has units of force per unit area, which later allows us to reconcile the surface forces on the body (per unit area) with the internal body forces (per unit volume).

Concerning the Cauchy's Stress Tensor, we have Cauchy's Fundamental Lemma (CFL), equivalent to Newton's 3rd law, which states

$$\sigma(x, y, z) \cdot \hat{n} = -\sigma(x, y, z) \cdot (-\hat{n}), \qquad \text{for any } \hat{n} \in \partial B(\hat{0}; 1) \text{ and } (x, y, z) \in \Omega,$$

where $\hat{0} = (0, 0, 0) \in \mathbb{R}^3$. The next lemma exploits CFL to show that the movement of the center of mass for a continuum body can be tracked only through external forces.

---

[3]Recall the deformation/displacement for a point particle, P, with initial position (x_0, y_0, z_0), at time t is defined as

$$u_P(t) = r_P(t) - r_P(0) \quad \text{or} \quad u(x_0, y_0, z_0, t) = (x_P(t), y_P(t), z_P(t)) - (x_0, y_0, z_0)$$

where $r_P(t) = (x_P(t), y_P(t), z_P(t))$ is the position of the particle at time t.

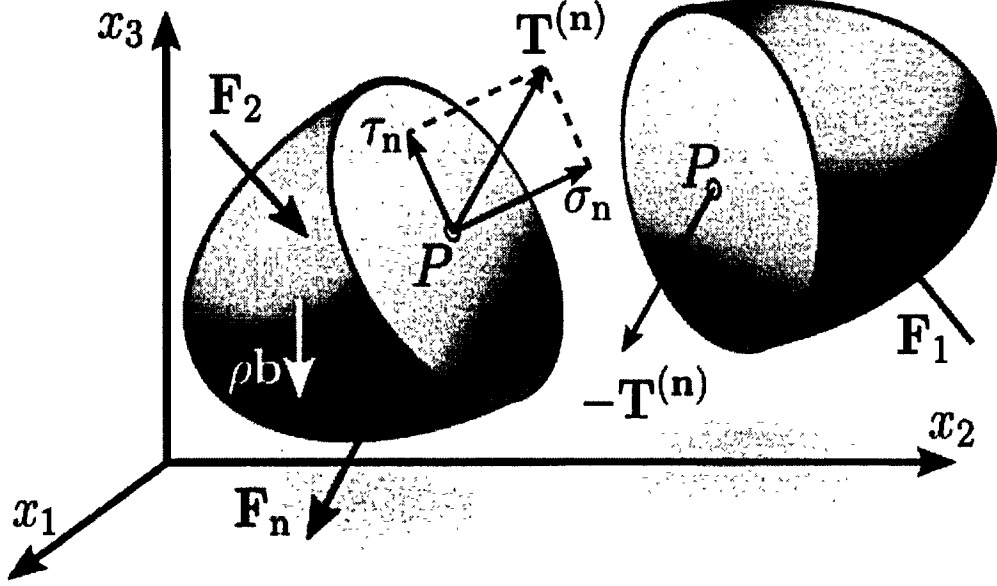[4]This Cauchy Stress "function" actually can be shown to be a tensor using Newton's 3rd Law.

Figure 1: Depiction of internal stress at point P by Sanpaz (own work) [CC BY-SA 3.0] (https://creativecommons.org/licenses/by-sa/3.0).

Lemma 3.1 *For a continuum body,* $\Omega \subset \mathbb{R}^3$, *with mass distribution,* $\rho : \Omega \to \mathbb{R}$ *under the influence of some external force distribution,* $f_e : \mathbb{R}^3 \to \mathbb{R}^3$, *then*

$$F_e = M\ddot{R},$$

where

$$F_e = \int_\Omega f_e \, dV, \quad M = \int_\Omega \rho \, dV, \quad and \quad \ddot{R} = \frac{1}{M} \int_\Omega \rho \ddot{r} \, dV.$$

Proof: Newton's 2nd (for mass distributions) states that for any point in the body

$$F(x, y, z) = \rho(x, y, z)\ddot{r}(x, y, z),$$

where $F(x, y, z)$ is the net force on $(x, y, z) \in \Omega$. In general,

$$F(x, y, z) = f_e(x, y, z) + \int_{\partial B(\hat{0};1)} T(\hat{n})(x, y, z) \, dS.$$

If we partition $\partial B(\hat{0};1) = \partial B^+(\hat{0};1) \cup \partial B^-(\hat{0};1), \partial B^+(\hat{0};1) \cap \partial B^-(\hat{0};1) = \varnothing$ such that

$$\hat{n} \in \partial B^+(\hat{0};1) \iff -\hat{n} \in \partial B^-(\hat{0};1),$$

8

then

$$\int_{\partial B(\hat{0};1)} T(\hat{n})(x,y,z)\,dS = \int_{\partial B^+(\hat{0};1)} T(\hat{n})(x,y,z)\,dS + \int_{\partial B^-(\hat{0};1)} T(\hat{n})(x,y,z)\,dS$$

$$= \int_{\partial B^+(\hat{0};1)} T(\hat{n})(x,y,z)\,dS + \int_{\partial B^+(\hat{0};1)} T(-\hat{n})(x,y,z)\,dS$$

$$= \int_{\partial B^+(\hat{0};1)} T(\hat{n})(x,y,z)\,dS - \int_{\partial B^+(\hat{0};1)} T(\hat{n})(x,y,z)\,dS \quad \text{[CFL]}$$

$$= \hat{0}$$

Therefore,

$$F_e = \int_\Omega f_e\,dV = \int_\Omega F\,dV = \int_\Omega \rho(x,y,z)\ddot{r}(x,y,z)\,dV = M\ddot{R}.$$

∎

3.2 Linear Elasticity Equations

Stress and strain are related through the rank 4 Stiffness Tensor, C. That is

$$\sigma(u) = C : \varepsilon(u), \qquad \text{or} \qquad \sigma_{ij} = C_{ijkl}\varepsilon_{kl}, \tag{2}$$

where (for isotropic solids)

$$C_{ijkl} = \lambda\delta_{ij}\delta_{kl} + \mu(\delta_{ik}\delta_{jl} + \delta_{il}\delta_{jk}),$$

and λ and μ are Lamé constants, particular to each material. At this point, it is imperative to emphasize some properties of C:

Lemma 3.2 *The following are properties of C:*

1. $C_{ijkl} = C_{jikl} = C_{ijlk} = C_{jilk}$ $\forall 1 \leq i,j,k,l \leq 3$.

2. $C_{ijkl} = 0$ for every $\{i,j,k,l\}$ such that any one index is different from the rest.

We leave it to the reader to verify the previously stated properties of C, as they are essential later in the process.

This relation guarantees the symmetry of σ for isotropic solids. Equation (2) can be interpreted as a "generalized Hooke's Law", and represents the most general statement about the linear relationship between the stresses on a body and the corresponding strains the former generate. At this point, we are ready to derive Cauchy's First Law of Motion:

Theorem 3.3 *For a continuum body, Ω, with mass distribution, ρ and stress tensor σ, under the influence of external inner body forces f_B (per unit volume) and surface traction forces f_S (per unit area), then*

$$\nabla \cdot \sigma + f_B = \rho\ddot{u}. \tag{3}$$

In particular, for static equilibrium $\ddot{u} = 0$.

9

Proof: Invoking the result from Lemma 3.1,

$$\int_{\partial\Omega} f_S \, dS + \int_\Omega f_B \, dV = \int_\Omega \rho \ddot{r} \, dV.$$

Now on the body's surface, $f_S = T(\hat{n})$, precisely with $\hat{n}$ as the unit normal vector at each point of the surface. Hence, by the divergence theorem

$$\int_{\partial\Omega} f_S \, dS = \int_{\partial\Omega} T(\hat{n}) \, dS = \int_{\partial\Omega} \sigma \cdot \hat{n} \, dS = \int_\Omega \nabla \cdot \sigma \, dV.$$

Also, it easily follows from their interrelated definition that $\ddot{r} = \ddot{u}$. So,

$$\int_\Omega \nabla \cdot \sigma \, dV + \int_\Omega f_B \, dV = \int_{\partial\Omega} f_S \, dS + \int_\Omega f_B \, dV = \int_\Omega \rho \ddot{r} \, dV = \int_\Omega \rho \ddot{u} \, dV$$

$$\implies \int_\Omega \nabla \cdot \sigma + f_B - \rho \ddot{u} \, dV = \hat{0}$$

$$\implies \nabla \cdot \sigma + f_B - \rho \ddot{u} = \hat{0} \qquad \text{[Arbitrary } \Omega\text{]}$$

$$\implies \nabla \cdot \sigma + f_B = \rho \ddot{u}$$

■

Suitable boundary conditions[5],

$$\begin{cases} \sigma \cdot \hat{n} = f_S \text{ on } S_f \\ u = u_S \text{ on } S_u \end{cases} \text{ with } \begin{cases} \partial\Omega = S_u \cup S_f \\ S_u \cap S_f = \varnothing \end{cases}, \tag{4}$$

yield a unique solution to (3). Unfortunately, however, it is extremely difficult, and in general not even possible, to solve the resulting PDE analytically, and hence we proceed with numerical methods.

3.3 Applying the FEM to CFLM

In this section, we will further specify the process involved in using the Finite Element Method, but with a particular focus on the problem at hand, namely Cauchy's First Law of Motion in the case for static equilibrium [4]. The procedure is as follows:

1. Partition Ω into a finite collection of nearly-disjoint elements, $\{K_i \subseteq \Omega\}_{i=1}^M$ (a.k.a. mesh), which only intersect at their boundaries:

$$\Omega = \bigcup_{i=1}^M K_i, \quad \text{and} \quad \mathring{K}_i \cap \mathring{K}_j = \varnothing, \text{ for } i \neq j.$$

---

[5]The fixed/known displacements, u_S, is called essential (or Dirichilet) boundary condition while the surface stresses, f_S, is called natural (Neumann) boundary condition.

10

2. Each element, K, is defined to contain a fixed number of nodes[6], $\{z_i\}_{i=1}^{N_i}$, with which one can define local nodal functions, $P_i^K : \Omega \to \mathbb{R}$, such that

$$P_i^K(z_j) = \begin{cases} 1, & \text{if } i = j \\ 0, & \text{if } i \neq j \end{cases}.$$

Nodal (a.k.a. shape) functions are typically polynomials. As a practical example, consider a two-dimensional rectangular cantilever, like in figure 2. In this case, each element is one of the adjoint rectangles, containing four nodes (the corners).
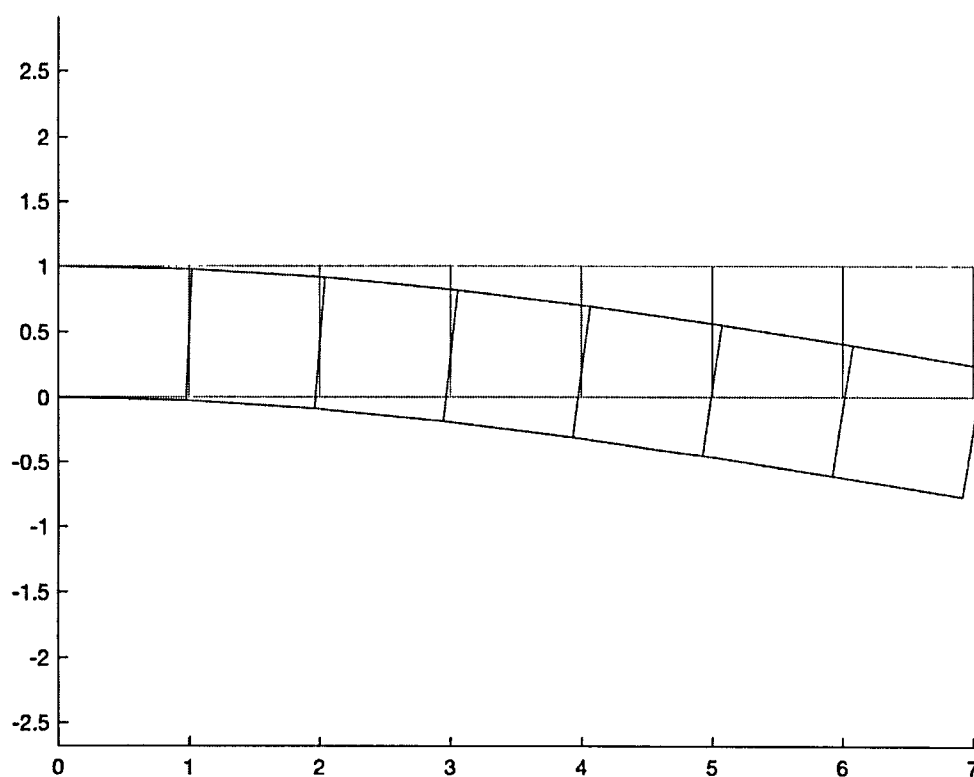

Figure 2: Discretized cantilever (green) and deformed body (red). Disregard the numbering on the axes, since it is irrelevant for this particular example.

---

[6]These are just evaluation points in the interior or boundary of the element.

3. Define global nodal functions, $\{P_j : \Omega \to \mathbb{R}\}_{j \in \Omega}$, by "pasting together" the P_i^K's which peak at the same node. Thus, the finite dimensional subspace, H, of the true solution space, X is the space of all continuous, piece-wise-component defined[7] functions on Ω. These are typically chosen to be polynomials, and further conditions can be imposed on the nodes in order to make these global functions differentiable up to any desired degree.

4. Approximate the solution to the elasticity PDE as an interpolation of the global shape functions in the following manner: If $u = (U, V, W)$, then

$$U = \sum_{j \in \Omega} U_j P_j; \qquad V = \sum_{j \in \Omega} V_j P_j; \qquad W = \sum_{j \in \Omega} W_j P_j.$$

Therefore, $\{P_j^{(d)} : d = 1, 2, 3 \text{ and } j \in \Omega\}$ where

$$P_j^{(1)} = (P_j, 0, 0); \qquad P_j^{(2)} = (0, P_j, 0); \qquad P_j^{(3)} = (0, 0, P_j)$$

is a basis for H.

5. Turn CFLM into the corresponding variational problem. We do this in the next theorem.

Theorem 3.4 (Principle of Virtual Displacements (PVD)) *Given a continuous body Ω satisfying (3) in static equilibrium with boundary conditions as in (4), then for any displacement function v such that $v = 0$ on S_u we have*

$$\int_\Omega \sigma(u) : \varepsilon(v) \, dV = \int_\Omega f_B \cdot v \, dV + \int_{S_f} f_S \cdot v \, dS.$$

Hence, in (1)

$$a(u, v) = \int_\Omega \sigma(u) : \varepsilon(v) \, dV \qquad and \qquad f = \begin{cases} f_B + f_S, & on \ S_f \\ f_B, & everywhere \ else \end{cases}.$$

Proof: Firstly,

$$\int_\Omega f_B \cdot v \, dV = \int_\Omega -(\nabla \cdot \sigma(u)) \cdot v \, dV \qquad \text{[Eq. (3) with } \ddot{u} = 0]$$

$$= \int_\Omega -\nabla \cdot (\sigma(u) \cdot v) \, dV + \int_\Omega (\sigma(u) : \nabla v) \, dV \qquad \text{[Lemma 2.1]}$$

$$= -\int_{\partial \Omega} (\sigma(u) \cdot v) \cdot \hat{n} \, dS + \int_\Omega (\sigma(u) : \nabla v) \, dV \qquad \text{[Divergence Theorem]}$$

---

[7]As in, piece-wise-component defined on each element and continuous over Ω.

Now,

$$\int_{\partial\Omega} (\sigma(u) \cdot v) \cdot \hat{n}\, dS = \int_{S_f} (\sigma(u) \cdot v) \cdot \hat{n}\, dS \qquad\qquad [v = 0 \text{ on } S_u]$$

$$= \int_{S_f} (\sigma(u) \cdot \hat{n}) \cdot v\, dS$$

$$= \int_{S_f} f_S \cdot v\, dS \qquad\qquad [\text{b.c. (4)}]$$

And also,

$$\int_{\Omega} (\sigma(u) : \nabla v)\, dV = \frac{1}{2} \left[\int_{\Omega} (\sigma(u) : \nabla v)\, dV + \int_{\Omega} (\sigma^{\mathrm{T}}(u) : \nabla^{\mathrm{T}} v)\, dV \right]$$

$$= \int_{\Omega} \frac{1}{2} (\sigma(u) : \nabla v + \sigma(u) : \nabla^{\mathrm{T}} v)\, dV \qquad\qquad [\sigma = \sigma^{\mathrm{T}}]$$

$$= \int_{\Omega} \sigma(u) : \varepsilon(v) \qquad\qquad [\text{Definition of } \varepsilon(v)]$$

Hence,

$$\int_{\Omega} \sigma(u) : \varepsilon(v)\, dV = \int_{\Omega} f_B \cdot v\, dV + \int_{S_f} f_S \cdot v\, dS,$$

as advertised. ∎

Remark 1: Due to their nature, certain surface forces (such as a hanging mass) are in practice treated as "point forces", and hence the surface integral can be split into two parts:

$$\int_{S_f} f_S \cdot v\, dS + \sum_i R_C^i \cdot v^i,$$

the left accounting for the "regular" force distribution across the body's surface, and the right representing the point forces, which have been integrated as delta-functions, and are therefore added.

Remark 2: We now explore the physical significance of the quadratic functional form of the PVD. The expression

$$\Pi(u) = a(u, u) - 2\langle f, u \rangle$$

$$= \int_{\Omega} \sigma(u) : \varepsilon(u)\, dV - 2\int_{\Omega} f_B \cdot u\, dV - 2\int_{S_f} f_S \cdot u\, dS - 2\sum_i R_C^i \cdot u^i \qquad (5)$$

actually stands for (twice) the total potential of the body. This implies that the solution to CFLM (and equivalently the PVD) minimizes the potential energy of the system, something which is most definitely expected when considering this scenario from a purely conceptual perspective. For this reason, the Principle of Virtual Displacements is also referred to as the Principle of Virtual Work (PVW).

13

6. Use the PVD and some compact notation exploiting the symmetry in ε and σ to generate and solve a (quite large) system of linear equations[8]

$$KU = R,$$

where K is called the stiffness matrix, U are the nodal displacements, and

$$R = R_B + R_S + R_C$$

represents the total nodal forces (inner body, surface, and concentrated loads, respectively). Because of the subtleties, we outline this specific step in further detail towards the end of the paper.

Remark 3: By the boundary conditions given in (4), we know the displacement of certain nodes (on S_u), for which we don't know the reactive forces, and we fully specified the forces on all other nodes (on $\mathring{\Omega}$ and S_f), for which the displacements are unknown, through f_B, f_S, and R_C. Therefore, to solve this system, one must first separate it in terms of the known and unknown quantities:

$$KU = R \implies \left[\begin{array}{c|c} K_{00} & K_{0x} \\ \hline K_{x0} & K_{xx} \end{array}\right] \cdot \left[\frac{U_0}{U_x}\right] = \left[\frac{R_0}{R_x}\right] \implies \begin{cases} K_{xx}U_x = R_x - K_{x0}U_0 \\ R_0 = K_{00}U_0 + K_{0x}U_x \end{cases},$$

where U_0 are the "fixed" displacement nodes on S_u, U_x are the free displacement nodes, R_0 are the reactive forces on S_u, and R_x are the known nodal forces.

Notice how this final linear system looks like a more complex form of Hooke's Law $F = kx$. In fact, in three dimensions, the scalar k becomes a tensor $\mathbb{K}$, such that

$$F = \left[\begin{array}{c} F_1 \\ F_2 \\ F_3 \end{array}\right] = \left[\begin{array}{ccc} \kappa_{11} & \kappa_{12} & \kappa_{13} \\ \kappa_{21} & \kappa_{22} & \kappa_{23} \\ \kappa_{31} & \kappa_{32} & \kappa_{33} \end{array}\right] \cdot \left[\begin{array}{c} X_1 \\ X_2 \\ X_3 \end{array}\right] = \mathbb{K} \cdot X.$$

Therefore, matrix K can be interpreted as the total stiffness of an idealized ensemble of node particles in which adjacent nodes i and j are connected by some 3D spring-like element with a stiffness tensor equal to the 3-by-3 submatrix, denoted K^{ij}.

Once the system is solved, then we have all the necessary coefficients to express the (approximated) solution in terms of the basis functions. If, $u_i = [U_i, V_i, W_i]^T$, we have that

$$u(x, y, x) = \sum_{j \in \Omega} u_j P_j(x, y, z).$$

Strains, stresses, and potential energy can then be calculated accordingly through the appropriate differentiation, product with the stiffness tensor, etc.

---

[8]In a case for which static equilibrium does not hold, similar arguments can be made to arrive at the final system

$$\Gamma \ddot{U} + KU = R,$$

where Γ is called the mass matrix of the system, obtained through integration the density term, ρ, and pairs of nodal functions. We include a brief commentary on this at the end of section 7.

4 Simulations

With all the mathematical theory polished and applied to the specific physical context, we programmed our own linear deformations software and ran a few simulations to test the accuracy and efficiency of our model, as well as to explore its limitations. We present the results of two of these simulations in the pages to follow.

4.1 Surface Strain Cantilever Experiment

The most important part of building a physical model is making sure it agrees with reality. In an attempt to verify the validity of our model, we simulated an experiment performed in a lab section of a Mechanics of Materials class of the Department of Civil Engineering at the University of Alabama in Huntsville (UAH) [5]. The purpose of the lab was to experimentally determine Young's modulus of elasticity for the given material as the slope of the graph of stress vs strain in the elastic region.

In this experiment, the students placed increasing/decreasing loads on one end of a 1.25 x 1 x 12.5 inch aluminum alloy (2024-T6) beam in a cantilever frame, and measured the resulting strain on the other end of the cantilever using a P-3500 strain indicator, as depicted in figure 3.
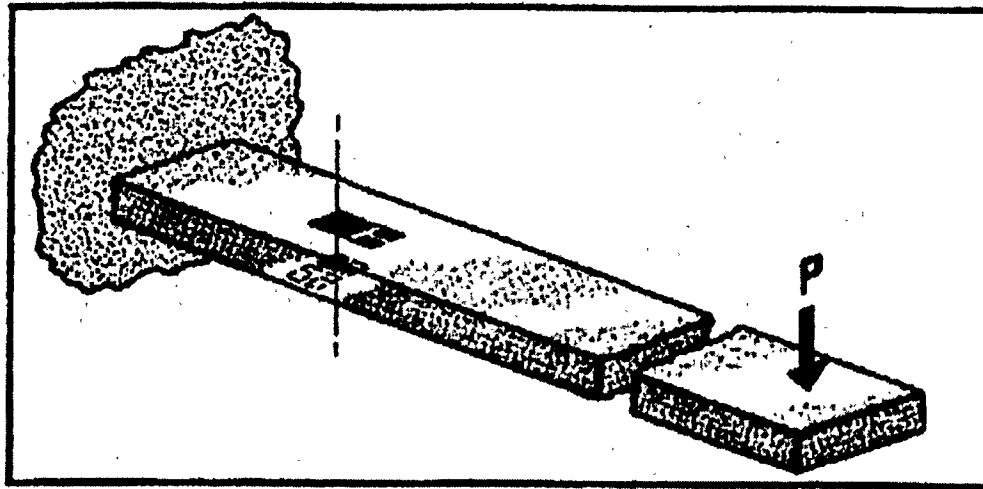

Figure 3: Strain cantilever experiment set-up.

The theoretical stress was obtained through a simplified stress equation which depends only on the applied load and the beam's geometry. The following data shows recorded strains for each applied load:

15

Load (lbs)	Measured Strain ($\mu\epsilon$)
0	0
0.22	88
0.44	175
0.66	262
0.88	350
1.10	435
1.32	523
1.54	611
1.76	695
1.98	782
2.2	870

The strains are obviously linear with respect to the loads mounted on the cantilever. For this reason, we began by checking that the strains our program outputted behaved in the same way. Figures 6 and 7 (located in the "Additional Figures" section at the end of the paper) are plots showing that, in our simulation, the surface strain at the point in which the sensor was located is indeed a linear function of the applied load on the other end of the cantilever. All calculations were done using a total of 100 elements (50 per length, 2 per width, and 1 per height)[9].

Another basic test we ran for this model was to check that the potential energy of the cantilever was a quadratic function of the applied force, something which clearly happens in a crude, one-dimensional spring:

$$\begin{cases} F = -ku \\ \Pi = \frac{1}{2}ku^2 \end{cases} \implies \Pi = \frac{1}{2k}F^2. \tag{6}$$

Figure 8 shows that, as we expected, the potential energy stored in the bent cantilever varies proportionally with the square of the applied force. This simulation was performed with the same 100 element mesh.

Up to this point, these tests have been mere "qualitative checks" which, though not directly related to the original purpose of the experiment, do help support the claim that the model agrees with reality. However, the vital part of this simulation was showing whether or not our program can estimate the measured strains within a reasonable degree of accuracy. Figures 9-12 show the surface strain computed in successive simulations as the mesh is refined[10] in the 0.22 lb load trial.

Although better refinements of the mesh clearly do improve the precision of the algorithm in a considerably, the successive strain approximations appear to "settle off" very

---

[9]You may notice that these calculations are significantly below the measured values, but no worries, for this will be discussed later on.

[10]This means that Ω is partitioned into an larger number of, necessarily "smaller", elements.

far away from (more that 30% below) the empirical value. Nevertheless, this initial disagreement between the two sets of data can be explained when considering the fact that the Young's Modulus of Elasticity empirically determined for the cantilever used in the lab experiment was 7.22 Mpsi, which is 31.2% lower than the established value for the 2024-T6 aluminum alloy (10.5 Mpsi).
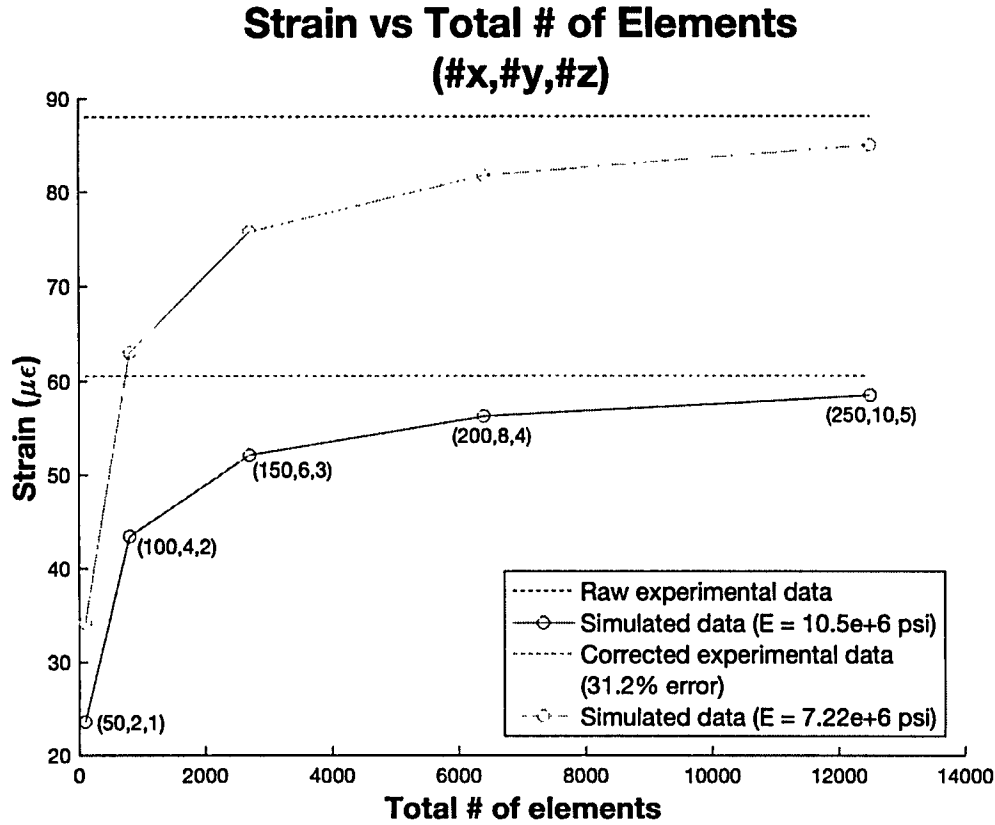

Figure 4: Surface strain approximations with mesh refinements in all directions for 0.22 lb load trial.

Therefore, the aluminum cantilever utilized in the lab was approximately 30% "less stiff" than regular aluminum 2024-T6 (that is $E_{exp} \approx 0.7 E_{act}$). So,

$$\begin{cases} E_{exp} = \dfrac{\Delta \sigma}{\Delta \varepsilon_{exp}} \\ E_{act} = \dfrac{\Delta \sigma}{\Delta \varepsilon_{act}} \end{cases} \implies \Delta \varepsilon_{exp} \approx \dfrac{1}{0.7} \Delta \varepsilon_{act}.$$

17

This means that, since the derived stresses were a function of only the beam's dimensions and the applied load, their measured strains would have been be about 30% larger than expected. When scaling their recorded values[11] by a factor of 30%, the simulations seem to converge quite nicely to the data from the experiment, as illustrated in figure 4, in the case for the 0.22 lb load. In fact, the horizontal lines representing the measured data even look like asymptotes for the estimated stresses.

4.2   Plane Stress vs Generalized 3D Model

Anything one would ever model is intrinsically three-dimensional, but complicated structures can only be modeled in 3D at a very high cost for memory and efficiency (speed). To circumvent this problem, under certain conditions, two- and even one-dimensional models can be utilized to obtain "good enough" approximations. One of such simplifications is the so-called "plane stress" condition, depicted in figure 5, which assumes that all the stresses on a body happen in a plane[12].
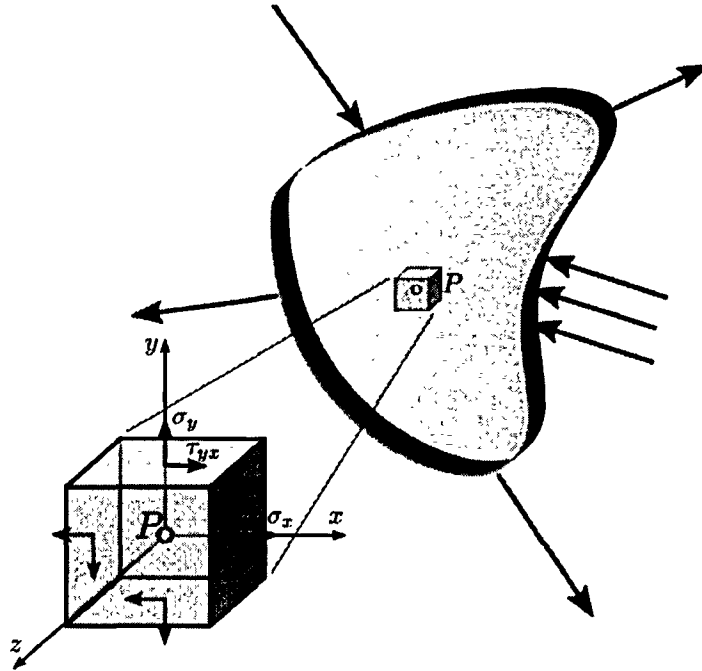

Figure 5:   Depiction of plane stress conditions by Sanpaz (own work) [CC BY-SA 3.0] (https://commons.wikimedia.org/w/index.php?curid=5717540).

---

[11]Or simulating a bar with a reduced Young's Modulus of Elasticity.

[12]Exploiting this geometry, said plane is typically made the xy-plane and hence, $\sigma_{ij} = 0$ for any $i, j = z$.

We now comment on some of the results of comparing a 2D (plane stress) and a 3D model for a (1 m x 10 cm) copper cantilever (bulk modulus $K = 123$ GPa and shear modulus $G = 45$ GPa), with one end fixed and the other under the pressure of a downward concentrated load on the other end. In both cases, the cantilevers were always partitioned along their length, with only one element per width and height.

In figure 13, we plotted the percent difference between the displacements generated in both models, each having the same number of elements, as a function of the bar's thickness (width). Notice that as the thickness increases, the 2D approximation approaches the 3D model, as we would expect. However, there seems to be an unavoidable 2-3% difference between these models.

For a different perspective on this same data, figure 14 shows the percent difference between the displacements calculated through each algorithm, but as a function of the number of elements in the mesh, with a fixed, common thickness. This graph shows that there exists some threshold thickness (between 0.1 and 0.01 (m)), above which mesh refinements only decrease the validity of a plane stress approximation, because the percent difference only grows larger. This data reinforces the great dependence of a good plane stress model on the initial assumption (i.e. stresses occur only in the plane).

Finally, we plotted the potential energy stored in the bent cantilevers as the mesh was refined (holding the thicknesses constant). In order the get comparable answers, the magnitude of the concentrated loads was scaled in proportion to the square root of the thickness, since rearranging equation (6), we obtain

$$F = \sqrt{2\Pi}\sqrt{k}.$$

Notice that, once again, the two-dimensional approximation, though it appears as if it were static, is actually approaching the three-dimensional model as the thickness decreases, but it can only get so close (about 2-3%).

5   Conclusions

5.1   Surface Strain Cantilever Experiment

This simulation seems to indicate that our model converges to empirical results as the mesh is refined. Although this is good news by itself, the necessity for extremely refined meshes in order to obtain "decent" approximations points at a more pressing concern. Like previously stated, a mesh refinement improves accuracy at a high cost for efficiency and memory space, therefore, it is only reasonable to develop some coherent error analysis theory to avoid unnecessary computations and optimize performance. Furthermore, our program, even in what can still be considered a rudimentary stage, could potentially be harnessed as a simple testing/calibration software for construction materials and lab equipment, since, in a way, we have already used it as such when analyzing the lab results.

5.2 Plane Stress vs Generalized 3D Model

In this experiment, we learned that there is a small, yet unshakeable, percent error difference (about 2-3%) between the displacements calculated with the plane stress and the generalized three-dimensional models. This could be due to the fact that any stresses involving the z-axis in the 2D approximation are simplified to be zero, but in reality, they never are. Relatively thin models exhibit very low stresses in the z-direction, which makes the approximation valid. Conversely, when the thickness grows larger, the effect of stresses in the z-direction is more pronounced in the 3D model, which makes the plane stress simplification invalid.

5.3 Future Research

In order to push this study forward, we distinguish three main areas of research:

- **Test the model further:**

  This can be done in a couple of different ways. The first is to compare our model to other structural analysis software that might be commercially available, like STAAD Pro. This will, hopefully, validate our model if our results match those obtained with other software, as well as point out areas of improvement or expansion. Also, the geometry of metal beams might be simple enough to attain an analytic solution to CFLM in this case. Exploring options like the Timoshenko or Euler-Bernoulli beam theories, could yield some sort of "real" solution to compare with our simulated approximations.

- **Expand the theoretical foundation of the model:**

  The data and results of our simulation, as previously stated, highlight the necessity of a rigorous error analysis theory. In practice, the goal would be to have some formula into which we could input some desired threshold accuracy to calculate the minimum number of elements in the mesh required to achieve said level of accuracy. In addition, since the end-goal is to model quantum systems, we may attempt, perhaps through some statistical analysis argument, to come up with some formula relating the true quantum behavior to the aggregate/classical behavior of a system of finite particles. Then, combining both of the previously mentioned error formulas, we can obtain an overall error bound between the results in our simulations and the true quantum behavior.

- **Enhance the applicability of the model:**

  In our original conversion of CFLM to its variational form, we assumed static equilibrium. The next logical step to make this model more applicable to diverse physical conditions would be turn the time-dependent version of the constitutive PDE into its variational form, which we actually do at the end of section 7, and then implement

20

it to code so we can test it and use it. After that, we can also try to develop a sort of "double" Finite Element Method in order to tackle the cantilever problem in the presence of an external electrostatic field. Then, the field itself can be approximated through a first FEM, which will specify the surface forces bending cantilever, and then a second FEM can be applied for the actual deformation part of the problem.

6 Acknowledgements

We would like to thank the Joy of Thinking organization at the University of Alabama in Huntsville and everyone involved in it for providing an invaluable environment for the learning and discussion of mathematics. We also want to thank, Micah Weaver, from the Civil Engineering Department at UAH, who was generous and humble enough to share his lab results with us. In addition, we would like to thank the UAH Physics Department for giving us the necessary motivation to begin this amazing endeavor.

7 Applying the FEM to CFLM (Continued)

In this section, we tie up a few loose ends concerning how to actually obtain the final system of equations to solve for the nodal displacements, as well as introduce new notation that will easy the implementation of the FEM into computer code. We will also say a few words on how to modify the system to account for inertial forces in the case that the loads are applied "rapidly"[13], and a truly dynamic (time-dependent) equation needs to be solved. That is, when $\rho \ddot{u} \neq 0$.

7.1 Obtaining the System $KU = R$

Recall that Theorem 3.4 proves

$$a(u,v) = \int_\Omega \sigma(u) : \varepsilon(v)\, dV, \qquad \text{and} \qquad f = \begin{cases} f_B + f_S, & \text{on } S_f \\ f_B, & \text{everywhere else} \end{cases}$$

is the variational form of the static equilibrium case of CFLM. Now, choosing some basis for $\mathbb{R}^3$, and applying part 1 of Lemma 3.2, we have

$$\sigma(u) : \varepsilon(v) = \sum_{i,j} \sigma(u)_{ij}\varepsilon(v)_{ij} = \sum_{i,j,k,l} C_{ijkl}\varepsilon(u)_{kl}\varepsilon(v)_{ij} = \sum_{i,j,k,l} C_{ijkl}\frac{1}{2}(u_{k,l} + u_{l,k})\frac{1}{2}(v_{i,j} + v_{j,i})$$

$$= \frac{1}{4}\left(\sum_{i,j,k,l} C_{ijkl}u_{k,l}v_{i,j} + \sum_{i,j,k,l} C_{ijkl}u_{l,k}v_{i,j} + \sum_{i,j,k,l} C_{ijkl}u_{k,l}v_{j,i} + \sum_{i,j,k,l} C_{ijkl}u_{l,k}v_{j,i}\right)$$

---

[13]That is, with respect to the natural frequency of the system.

$$= \frac{1}{4}\left(\sum_{i,j,k,l} C_{ijkl}u_{k,l}v_{i,j} + \sum_{i,j,k,l} C_{ijlk}u_{l,k}v_{i,j} + \sum_{i,j,k,l} C_{jikl}u_{k,l}v_{j,i} + \sum_{i,j,k,l} C_{jilk}u_{l,k}v_{j,i}\right)$$

$$= \sum_{i,j,k,l} C_{ijkl}u_{k,l}v_{i,j}$$

Next, using part 2 of Lemma 3.2, we derive all the possible combinations for $a\left(P_n^{(\alpha)}, P_m^{(\beta)}\right)$, corresponding to nodes n and m:

$$a\left(P_n^{(1)}, P_m^{(1)}\right) = \int_\Omega \tau\left(P_n^{(1)}\right) : \varepsilon\left(P_m^{(1)}\right) dV = \int_\Omega \sum_{i,j,k,l} C_{ijkl}\left(P_n^{(1)}\right)_{k,l}\left(P_m^{(1)}\right)_{i,j} dV$$

$$= \int_\Omega \sum_{k,l} C_{1j1l}\left(\frac{\partial P_n}{\partial x_l}\right)\left(\frac{\partial P_m}{\partial x_j}\right) dV$$

$$= \int_\Omega C_{1111}\left(\frac{\partial P_n}{\partial x}\right)\left(\frac{\partial P_m}{\partial x}\right) + C_{1212}\left(\frac{\partial P_n}{\partial y}\right)\left(\frac{\partial P_m}{\partial y}\right) + C_{1313}\left(\frac{\partial P_n}{\partial z}\right)\left(\frac{\partial P_m}{\partial z}\right) dV$$

$$a\left(P_n^{(1)}, P_m^{(2)}\right) = \int_\Omega \tau\left(P_n^{(1)}\right) : \varepsilon\left(P_m^{(2)}\right) dV = \int_\Omega \sum_{i,j,k,l} C_{ijkl}\left(P_n^{(1)}\right)_{k,l}\left(P_m^{(2)}\right)_{i,j} dV$$

$$= \int_\Omega \sum_{k,l} C_{1j2l}\left(\frac{\partial P_n}{\partial x_l}\right)\left(\frac{\partial P_m}{\partial x_j}\right) dV$$

$$= \int_\Omega C_{1122}\left(\frac{\partial P_n}{\partial y}\right)\left(\frac{\partial P_m}{\partial x}\right) + C_{1221}\left(\frac{\partial P_n}{\partial x}\right)\left(\frac{\partial P_m}{\partial y}\right) dV$$

$$a\left(P_n^{(1)}, P_m^{(3)}\right) = \int_\Omega \tau\left(P_n^{(1)}\right) : \varepsilon\left(P_m^{(3)}\right) dV = \int_\Omega \sum_{i,j,k,l} C_{ijkl}\left(P_n^{(1)}\right)_{k,l}\left(P_m^{(3)}\right)_{i,j} dV$$

$$= \int_\Omega \sum_{k,l} C_{1j3l}\left(\frac{\partial P_n}{\partial x_l}\right)\left(\frac{\partial P_m}{\partial x_j}\right) dV$$

$$= \int_\Omega C_{1133}\left(\frac{\partial P_n}{\partial z}\right)\left(\frac{\partial P_m}{\partial x}\right) + C_{1331}\left(\frac{\partial P_n}{\partial x}\right)\left(\frac{\partial P_m}{\partial z}\right) dV$$

$$a\left(P_n^{(2)}, P_m^{(1)}\right) = \int_\Omega \tau\left(P_n^{(2)}\right) : \varepsilon\left(P_m^{(1)}\right) = \int_\Omega \sum_{i,j,k,l} C_{ijkl}\left(P_n^{(2)}\right)_{k,l}\left(P_m^{(1)}\right)_{i,j} dV$$

$$= \int_\Omega \sum_{k,l} C_{2j1l}\left(\frac{\partial P_n}{\partial x_l}\right)\left(\frac{\partial P_m}{\partial x_j}\right) dV$$

$$= \int_\Omega C_{2211}\left(\frac{\partial P_n}{\partial x}\right)\left(\frac{\partial P_m}{\partial y}\right) + C_{2112}\left(\frac{\partial P_n}{\partial y}\right)\left(\frac{\partial P_m}{\partial x}\right) dV$$

$$a\left(P_n^{(2)}, P_m^{(2)}\right) = \int_\Omega \tau\left(P_n^{(2)}\right) : \varepsilon\left(P_m^{(2)}\right) dV = \int_\Omega \sum_{i,j,k,l} C_{ijkl} \left(P_n^{(2)}\right)_{k,l} \left(P_m^{(2)}\right)_{i,j} dV$$

$$= \int_\Omega \sum_{k,l} C_{2j2l} \left(\frac{\partial P_n}{\partial x_l}\right)\left(\frac{\partial P_m}{\partial x_j}\right) dV$$

$$= \int_\Omega C_{2121}\left(\frac{\partial P_n}{\partial x}\right)\left(\frac{\partial P_m}{\partial x}\right) + C_{2222}\left(\frac{\partial P_n}{\partial y}\right)\left(\frac{\partial P_m}{\partial y}\right) + C_{2323}\left(\frac{\partial P_n}{\partial z}\right)\left(\frac{\partial P_m}{\partial z}\right) dV$$

$$a\left(P_n^{(2)}, P_m^{(3)}\right) = \int_\Omega \tau\left(P_n^{(2)}\right) : \varepsilon\left(P_m^{(3)}\right) dV = \int_\Omega \sum_{i,j,k,l} C_{ijkl} \left(P_n^{(2)}\right)_{k,l} \left(P_m^{(3)}\right)_{i,j} dV$$

$$= \int_\Omega \sum_{k,l} C_{2j3l} \left(\frac{\partial P_n}{\partial x_l}\right)\left(\frac{\partial P_m}{\partial x_j}\right) dV$$

$$= \int_\Omega C_{2233}\left(\frac{\partial P_n}{\partial z}\right)\left(\frac{\partial P_m}{\partial y}\right) + C_{2332}\left(\frac{\partial P_n}{\partial y}\right)\left(\frac{\partial P_m}{\partial z}\right) dV$$

$$a\left(P_n^{(3)}, P_m^{(1)}\right) = \int_\Omega \tau\left(P_n^{(3)}\right) : \varepsilon\left(P_m^{(1)}\right) dV = \int_\Omega \sum_{i,j,k,l} C_{ijkl} \left(P_n^{(3)}\right)_{k,l} \left(P_m^{(1)}\right)_{i,j} dV$$

$$= \int_\Omega \sum_{k,l} C_{3j1l} \left(\frac{\partial P_n}{\partial x_l}\right)\left(\frac{\partial P_m}{\partial x_j}\right) dV$$

$$= \int_\Omega C_{3311}\left(\frac{\partial P_n}{\partial x}\right)\left(\frac{\partial P_m}{\partial z}\right) + C_{3113}\left(\frac{\partial P_n}{\partial z}\right)\left(\frac{\partial P_m}{\partial x}\right)$$

$$a\left(P_n^{(3)}, P_m^{(2)}\right) = \int_\Omega \tau\left(P_n^{(3)}\right) : \varepsilon\left(P_m^{(2)}\right) dV = \int_\Omega \sum_{i,j,k,l} C_{ijkl} \left(P_n^{(3)}\right)_{k,l} \left(P_m^{(2)}\right)_{i,j} dV$$

$$= \int_\Omega \sum_{k,l} C_{3j2l} \left(\frac{\partial P_n}{\partial x_l}\right)\left(\frac{\partial P_m}{\partial x_j}\right) dV$$

$$= \int_\Omega C_{3322}\left(\frac{\partial P_n}{\partial y}\right)\left(\frac{\partial P_m}{\partial z}\right) + C_{3223}\left(\frac{\partial P_n}{\partial z}\right)\left(\frac{\partial P_m}{\partial y}\right) dV$$

$$a\left(P_n^{(3)}, P_m^{(3)}\right) = \int_\Omega \tau\left(P_n^{(3)}\right) : \varepsilon\left(P_m^{(3)}\right) dV = \int_\Omega \sum_{i,j,k,l} C_{ijkl} \left(P_n^{(3)}\right)_{k,l} \left(P_m^{(3)}\right)_{i,j} dV$$

$$= \int_\Omega \sum_{k,l} C_{3j3l} \left(\frac{\partial P_n}{\partial x_l}\right)\left(\frac{\partial P_m}{\partial x_j}\right) dV$$

$$= \int_\Omega C_{3131}\left(\frac{\partial P_n}{\partial x}\right)\left(\frac{\partial P_m}{\partial x}\right) + C_{3232}\left(\frac{\partial P_n}{\partial y}\right)\left(\frac{\partial P_m}{\partial y}\right) + C_{3333}\left(\frac{\partial P_n}{\partial z}\right)\left(\frac{\partial P_m}{\partial z}\right) dV$$

It is worth pointing out all the possible values of C_{ijkl}:

$$C_{ijkl} = \begin{cases} \lambda + 2\mu, & \text{if } i = j = k = l \\ \lambda, & \text{if } i = j \neq k = l \\ \mu, & \text{if } i = k \neq j = l \text{ or } i = l \neq j = k \end{cases}$$

So, if Ω contains a total of N nodes, each pair of elements, (n, m), defines a 3-by-3 submatrix, K^{nm}, in which the element $K_{\alpha\beta}^{nm}$ is $a\left(P_n^{(\alpha)}, P_m^{(\beta)}\right)$. Finally, K becomes

$$K = \begin{bmatrix} K^{11} & K^{12} & \cdots & K^{1m} & \cdots & K^{1N} \\ K^{11} & K^{12} & \cdots & K^{2m} & \cdots & K^{2N} \\ \vdots & \vdots & \ddots & & & \\ K^{n1} & K^{n2} & & K^{nm} & \cdots & K^{nN} \\ \vdots & \vdots & & \vdots & \ddots & \\ K^{N1} & K^{N2} & & K^{Nm} & & K^{NN} \end{bmatrix}.$$

It's worth noting that the respective integrations over Ω for each submatrix are not coupled and thus need not be performed in the global coordinate system, X, Y, Z, but can be done in some local coordinate system, x_m, y_m, z_m, for each element m.

Lastly, the coefficients vector, U, becomes

$$U = \begin{bmatrix} U_1 & V_1 & W_1 & U_2 & V_2 & W_2 & \cdots & U_N & V_N & W_N \end{bmatrix}^{\mathrm{T}},$$

while the nodal forces vector, R, can be decomposed as

$$R = R_B + R_S + R_C,$$

where

$$R_B = \left[(R_B)_1^{(1)} (R_B)_1^{(2)} (R_B)_1^{(3)} \quad (R_B)_2^{(1)} (R_B)_2^{(2)} (R_B)_2^{(3)} \quad \cdots \quad (R_B)_N^{(1)} (R_B)_N^{(2)} (R_B)_N^{(3)} \right]^{\mathrm{T}}$$

with $\quad (R_B)_n^{(\alpha)} = \int_\Omega f_B \cdot P_n^{(\alpha)} \, dV,$

24

$$R_S = \left[(R_S)_1^{(1)}(R_S)_1^{(2)}(R_S)_1^{(3)} \quad (R_S)_2^{(1)}(R_S)_2^{(2)}(R_S)_2^{(3)} \quad \cdots \quad (R_S)_N^{(1)}(R_S)_N^{(2)}(R_S)_N^{(3)}\right]^{\mathrm{T}}$$

$$\text{with} \quad (R_S)_n^{(\alpha)} = \int_\Omega f_S \cdot P_n^{(\alpha)} \, dV,$$

$$R_C = \left[(R_C)_1^{(1)}(R_C)_1^{(2)}(R_C)_1^{(3)} \quad (R_C)_2^{(1)}(R_C)_2^{(2)}(R_C)_2^{(3)} \quad \cdots \quad (R_C)_N^{(1)}(R_C)_N^{(2)}(R_C)_N^{(3)}\right]^{\mathrm{T}},$$

and $(R_C)_n^{(\alpha)}$ is the α component of the concentrated load acting on node n. And with that, we have fully constructed the system $KU = R$ for static equilibrium.

7.2 Programming-friendly Notation

For programming purposes, it turns out that the symmetry of τ, ε, and C give us a systematic way of computing, K^{nm}, through a simple matrix product:

$$K^{nm} = \int_\Omega B_n^{\mathrm{T}} E B_m \, dV,$$

where the integration is understood to be for each entry individually,

$$E = \begin{bmatrix} \lambda+2\mu & \lambda & \lambda & 0 & 0 & 0 \\ \lambda & \lambda+2\mu & \lambda & 0 & 0 & 0 \\ \lambda & \lambda & \lambda+2\mu & 0 & 0 & 0 \\ 0 & 0 & 0 & \mu & 0 & 0 \\ 0 & 0 & 0 & 0 & \mu & 0 \\ 0 & 0 & 0 & 0 & 0 & \mu \end{bmatrix}, \quad \text{and} \quad B_n = \begin{bmatrix} \dfrac{\partial P_n}{\partial x} & 0 & 0 \\ 0 & \dfrac{\partial P_n}{\partial y} & 0 \\ 0 & 0 & \dfrac{\partial P_n}{\partial z} \\ \dfrac{\partial P_n}{\partial y} & \dfrac{\partial P_n}{\partial x} & 0 \\ 0 & \dfrac{\partial P_n}{\partial z} & \dfrac{\partial P_n}{\partial y} \\ \dfrac{\partial P_n}{\partial z} & 0 & \dfrac{\partial P_n}{\partial x} \end{bmatrix}.$$

We have already mentioned that the integration can occur in local coordinates, though in practice, it is convenient to resort to some clever parameterization taking into account each element's geometry. Typically, for an element m, the local coordinates, x_m, y_m, z_m, are converted into "intrinsic" (a.k.a. "natural") coordinates, r_m, s_m, t_m. Now, along with this change of coordinates comes a Jacobian, J, to perform the integration, and an inverse

Jacobian, J^{-1}, to transform the derivative terms that appear in the integrand:

$$J = \begin{bmatrix} \dfrac{\partial x_m}{\partial r_m} & \dfrac{\partial y_m}{\partial r_m} & \dfrac{\partial z_m}{\partial r_m} \\[2ex] \dfrac{\partial x_m}{\partial s_m} & \dfrac{\partial y_m}{\partial s_m} & \dfrac{\partial z_m}{\partial s_m} \\[2ex] \dfrac{\partial x_m}{\partial t_m} & \dfrac{\partial y_m}{\partial t_m} & \dfrac{\partial z_m}{\partial t_m} \end{bmatrix}, \quad \text{and} \quad J^{-1} = \begin{bmatrix} \dfrac{\partial r_m}{\partial x_m} & \dfrac{\partial s_m}{\partial x_m} & \dfrac{\partial t_m}{\partial x_m} \\[2ex] \dfrac{\partial r_m}{\partial y_m} & \dfrac{\partial s_m}{\partial y_m} & \dfrac{\partial t_m}{\partial y_m} \\[2ex] \dfrac{\partial r_m}{\partial z_m} & \dfrac{\partial s_m}{\partial z_m} & \dfrac{\partial t_m}{\partial z_m} \end{bmatrix}.$$

At this stage, one can use numerical integration methods to perform all the appropriate integrals. For example, a Gaussian quadrature scheme would turn each definite integral into a summation,

$$K^{nm} = \int_\Omega B_n^{\mathrm{T}} E B_m \, dV = \sum_{i,j,k} \omega_{ijk} \Lambda_{ijk},$$

where Λ_{ijk} are evaluations of $B_n^{\mathrm{T}} E B_m \det(J)$ at specific points, and ω_{ijk} are the corresponding weights.

Lastly, this same matrix notation and the embedded symmetry of these operators allow us to express all six distinct components of the strain and stress functions, as well as the estimated potential energy, $\bar{\Pi}$, by

$$\begin{bmatrix} \varepsilon_{xx} \\ \varepsilon_{yy} \\ \varepsilon_{zz} \\ \gamma_{xy} \\ \gamma_{yz} \\ \gamma_{xz} \end{bmatrix} = \sum_{i \in \Omega} B_i u_i; \qquad \begin{bmatrix} \sigma_{xx} \\ \sigma_{yy} \\ \sigma_{zz} \\ \sigma_{xy} \\ \sigma_{yz} \\ \sigma_{xz} \end{bmatrix} = \sum_{i \in \Omega} E B_i u_i; \quad \text{and} \quad \bar{\Pi} = \frac{1}{2} U^{\mathrm{T}} K U = \frac{1}{2} U^{\mathrm{T}} R,$$

where $\gamma_{ij} = 2\varepsilon_{xy}$ are called the engineering shear-strains and $u_i = [U_i, V_i, W_i]^{\mathrm{T}}$ as previously described in the paper.

7.3 Time-dependent CFLM

In the case for which static equilibrium does not hold (i.e. $\rho\ddot{u} \neq 0$), a re-derivation of the PVD yields that

$$a(u, v) = \int_\Omega \rho\ddot{u} \cdot v \, dV + \int_\Omega \sigma(u) : \varepsilon(v) \, dV.$$

The acceleration terms is decomposed similarly: $\ddot{u} = (\ddot{U}, \ddot{V}, \ddot{W})$, with

$$\ddot{U} = \sum_{j \in \Omega} \ddot{U}_j P_j; \qquad \ddot{V} = \sum_{j \in \Omega} \ddot{V}_j P_j; \qquad \ddot{W} = \sum_{j \in \Omega} \ddot{W}_j P_j.$$

26

Then, the same procedure changes the original system to

$$\Gamma \ddot{U} + KU = R,$$

where

$$\ddot{U} = \begin{bmatrix} \ddot{U}_1 & \ddot{V}_1 & \ddot{W}_1 & \ddot{U}_2 & \ddot{V}_2 & \ddot{W}_2 & \cdots & \ddot{U}_N & \ddot{V}_N & \ddot{W}_N \end{bmatrix}^{\mathrm{T}},$$

and

$$\Gamma = \begin{bmatrix} \Gamma^{11} & \Gamma^{12} & \cdots & \Gamma^{1m} & \cdots & \Gamma^{1N} \\ \Gamma^{11} & \Gamma^{12} & \cdots & \Gamma^{2m} & \cdots & \Gamma^{2N} \\ \vdots & \vdots & \ddots & & & \\ \Gamma^{n1} & \Gamma^{n2} & & \Gamma^{nm} & \cdots & \Gamma^{nN} \\ \vdots & \vdots & & \vdots & \ddots & \\ \Gamma^{N1} & \Gamma^{N2} & & \Gamma^{Nm} & & \Gamma^{NN} \end{bmatrix}.$$

Each 3-by-3 submatrix is defined as

$$\Gamma^{nm}_{\alpha\beta} = \int_\Omega \rho P_n^{(\alpha)} \cdot P_m^{(\beta)} \, dV,$$

and all other terms (K, U, and R) are the same as previously described. Same as before, the corresponding system should be separated according to the boundary conditions specified,

$$\Gamma \ddot{U} + KU = R \implies \begin{bmatrix} \Gamma_{00} & \Gamma_{0x} \\ \Gamma_{x0} & \Gamma_{xx} \end{bmatrix} \cdot \begin{bmatrix} \ddot{U}_0 \\ \ddot{U}_x \end{bmatrix} + \begin{bmatrix} K_{00} & K_{0x} \\ K_{x0} & K_{xx} \end{bmatrix} \cdot \begin{bmatrix} U_0 \\ U_x \end{bmatrix} = \begin{bmatrix} R_0 \\ R_x \end{bmatrix},$$

and then solved using a method of choice.
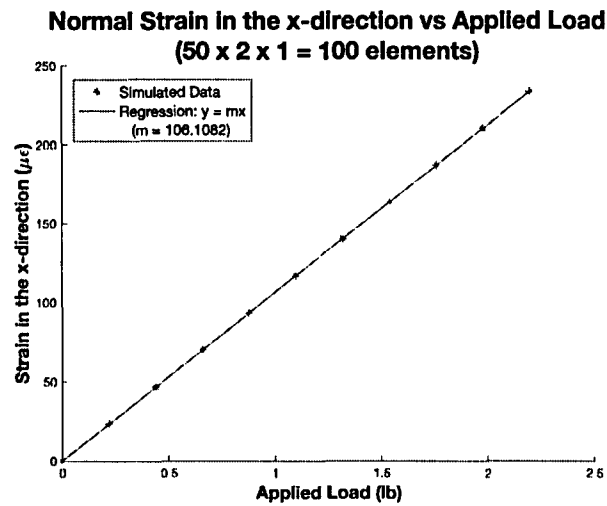
27

8 Additional Figures

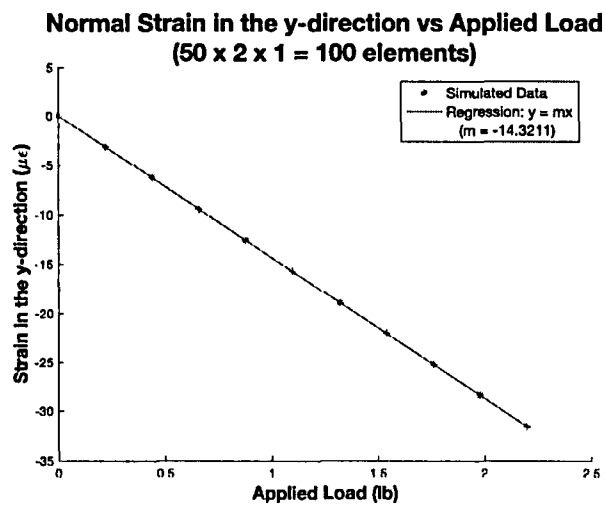Figure 6: Simulated strain in the x-direction vs the applied load.

Figure 7: Simulated strain in the y-direction vs the applied load.
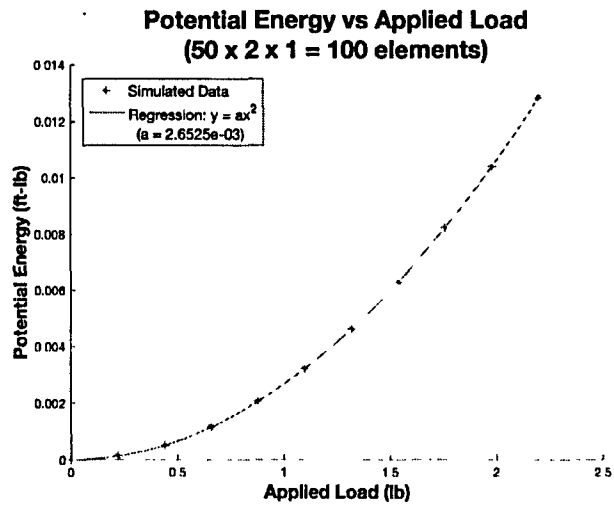
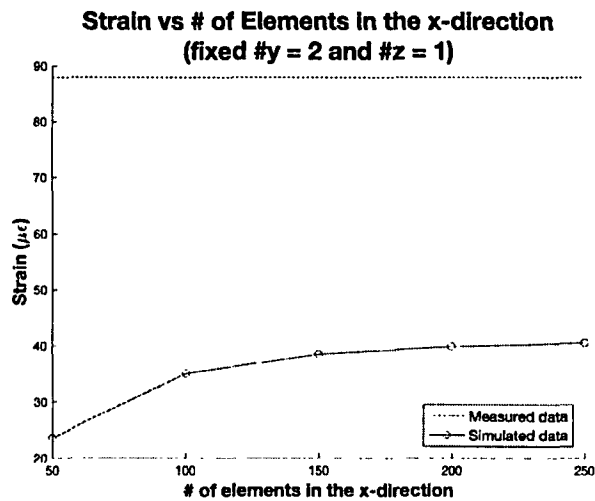Figure 8: Potential energy is a quadratic function of the applied load.

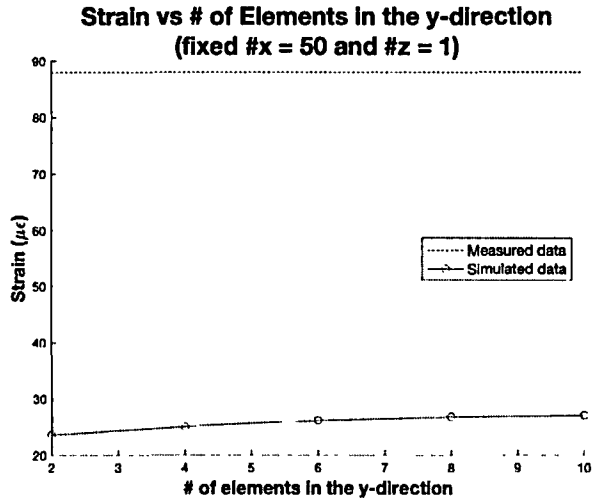Figure 9: Surface strain approximations with mesh refinements in x-direction for 0.22 lb load trial.

29

Strain vs # of Elements in the y-direction
(fixed #x = 50 and #z = 1)

Figure 10: Surface strain approximations with mesh refinements in y-direction for 0.22 lb load trial.

Strain vs # of Elements in the z-direction
(fixed #x = 50 and #y = 2)
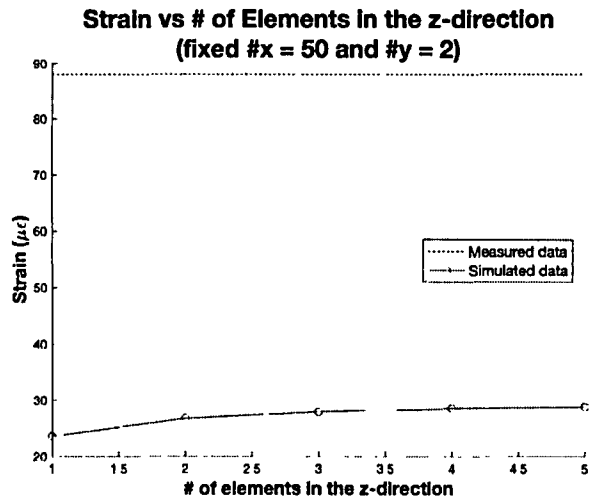
Figure 11: Surface strain approximations with mesh refinements in z-direction for 0.22 lb load trial.
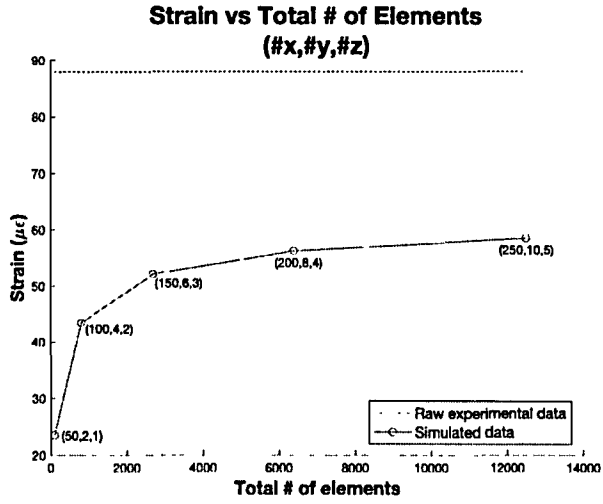
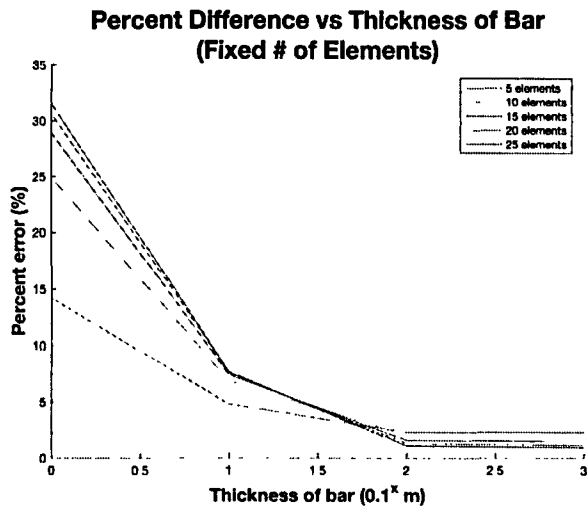**Figure 12:** Surface strain approximations with mesh refinements in all directions for 0.22 lb load trial.

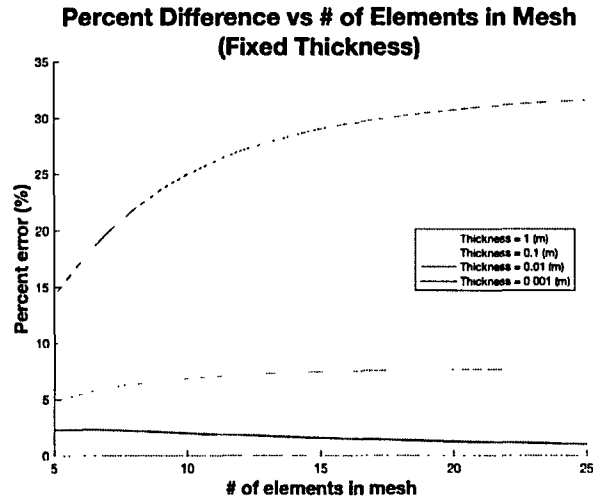**Figure 13:** Percent difference on displacements at several thicknesses for the bar with a fixed number of elements.

Percent Difference vs # of Elements in Mesh
(Fixed Thickness)

Figure 14: Percent difference on displacements for a range of total elements with fixed thicknesses.

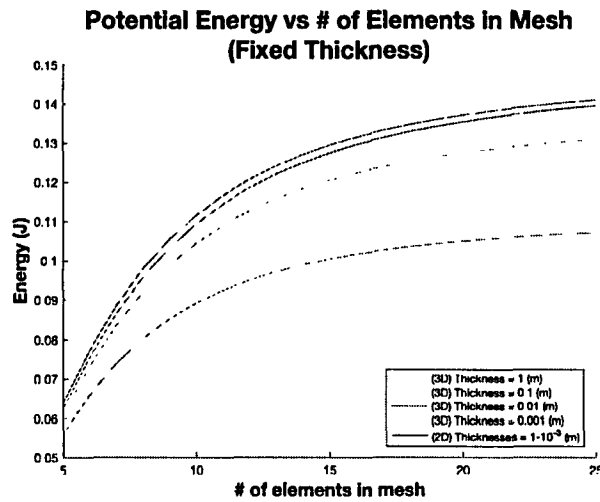**Potential Energy vs # of Elements in Mesh**
(Fixed Thickness)

Figure 15: Potential energies vs number of elements at fixed thicknesses. Load was varied proportionally to the square root of the thickness.

32

References

[1] William G. Strang and George J Fix. *An Analysis of the Finite Element Method.* Englewood Cliffs, N.J., Prentice Hall, 1973.

[2] Susanne C. Brenner and L. Ridgway Scott. *The Mathematical Theory of Finite Element Methods.* Springer Science, 3rd edition, 2008.

[3] W. Michael Lai, David Rubin, and Erhand Krempl. *Introduction to Continuum Mechanics.* Elsevier Inc., 4th edition, 2010.

[4] Klaus-Jürgen Bathe. *Finite Element Procedures.* Prentice Hall, Pearson Education, Inc., 2nd edition, 2014.

[5] Micah Weaver. Lab 02: Modulus of elasticity flexure test. MAE 370 Lab Report, September 2017.